Development of an endothelial cell restricted transgenic reporter rat: A resource for physiological studies of vascular biology

Mikhail Alexeyev[1,6,^], Aron M. Geurts[7,^], Naga S. Annamdevula[2,6,^], C. Michael Francis[1,6,^], Silas Leavesley[3,6], Thomas Rich[2,6], Mark S. Taylor[1,6], Mike Lin[1,6], Ron Balczon[4,6], Jennifer Knighten[1], Diego F. Alvarez[8,*], and Troy Stevens[1,5,6,*]

^ denotes equal contribution(s); * denotes corresponding author(s)

Departments of Physiology and Cell Biology[1], Pharmacology[2], Chemical and Biomolecular Engineering[3], Biochemistry and Molecular Biology[4], Internal Medicine[5], the Center for Lung Biology[6], University of South Alabama, Mobile, AL 36688, USA; Genome Editing Rat Resource Center[7], Department of Physiology, Medical College of Wisconsin, Milwaukee, WI 53226, USA; Department of Physiology and Pharmacology[8], College of Osteopathic Medicine, Conroe, TX 77304, USA

Corresponding Author(s):
Troy Stevens, Ph.D.
Lenoire Louise Locke Professor and Chair
Departments of Physiology and Cell Biology and Internal Medicine
Director, Center for Lung Biology
University of South Alabama
Mobile, AL 36688
Phone: (251) 460-6056
Fax: (251) 460-7452
Email: tstevens@southalabama.edu

Diego Alvarez, M.D., Ph.D.
Associate Professor and Chair
Department of Physiology and Pharmacology
College of Osteopathic Medicine
Sam Houston State University
Conroe, TX 77304
Phone: (936) 202-5213
Fax: (936) 294-4399
Email: diego.alvarez@shsu.edu

Running Title: Endothelial-restricted reporter rat model

New and noteworthy: Transgenic mice have been instrumental in advancing molecular insight of physiological processes, yet these models oftentimes do not faithfully recapitulate human physiology and pathophysiology. Rat models better replicate some human conditions, like Group 1 pulmonary arterial hypertension. Here, we report the development of an endothelial cell restricted transgenic reporter rat that has broad application to vascular biology. This first-in-kind model offers exceptional endothelial restricted tdTomato expression, in both conduit vessels and the microcirculations of organs.

Keywords:

(1) CDH5 (VE-cadherin)

(2) Cre recombinase (iCre)

(3) tdTomato

(4) Animal model

(5) Pulmonary hypertension

Abstract

Here, we report the generation of a Cre-recombinase transgenic rat, where iCre is driven using a CDH5 promoter. The CDH5 promoter was cloned from rat pulmonary microvascular endothelial cells and demonstrated approximately 60% similarity to the murine counterpart. The cloned rat promoter was 2,508 bp, it extended 79 bp beyond the transcription start site, and it was 22,923 bp upstream of the translation start site. The novel promoter was cloned upstream of codon-optimized iCre and subcloned into a *Sleeping Beauty* transposon vector for transpositional transgenesis in Sprague-Dawley rats. Transgenic founders were generated and selected for iCre expression. Crossing the CDH5-iCre rat with a tdTomato reporter rat resulted in progeny displaying endothelial-restricted fluorescence. tdTomato fluorescence was prominent in major arteries and veins, and it was similar in males and females. Quantitative analysis of the carotid artery and the jugular vein revealed that on average more than 50% of the vascular surface area exhibited strong fluorescence. tdTomato fluorescence was observed in the circulations of every tissue tested. The microcirculation in all tissues tested displayed homogenous fluorescence. Fluorescence was examined across young (6-7.5 months), middle (14-16.5 months), and old age (17-19.5 months) groups. Although tdTomato fluorescence was seen in middle- and old-age animals, the intensity of the fluorescence was significantly reduced compared to that seen in the young rats. Thus, this endothelial restricted transgenic rat offers a novel platform to test endothelial microheterogeneity within all vascular segments and it provides exceptional resolution of endothelium within organ microcirculations for application to translational disease models.

Introduction

Endothelium forms a highly dynamic barrier that coordinates the passage of water, solutes, macromolecules and cells between the blood and the underlying tissue. Endothelial cells are highly specialized, or differentiated, to achieve the functions of any given vascular location(2, 14). Such differentiation is classified on an anatomical basis, being either continuous, discontinuous or fenestrated(2). Conduit vessels, like the carotid artery and jugular vein, and capillaries in organs like the skin, lung, central nervous system, and muscle, possess a continuous type of endothelium, where cells reside on an underlying basement membrane. Organs like the liver, spleen, and bone marrow possess a discontinuous, or sinusoidal-type, capillary endothelium, where the cells do not reside on a basement membrane. The kidney glomerulus, endocrine glands and intestinal endothelium each exhibits fenestrae, which are contiguous transcellular openings. These anatomical classifications relate to the variable ability of endothelium to regulate permeability in accordance with site-specific environmental demands. Permeability of the continuous endothelium largely occurs through intercellular junctions, and to a lesser degree, through vesicular transcytosis, both of which are highly regulated processes(23, 30, 31). Physiological stimuli dynamically adjust the strength of cell-to-cell junctions and the rate of transcytosis in order to coordinate blood-to-tissue communication. In contrast to this process, discontinuous endothelium offers less resistance to permeability and fenestrated endothelium serves to sieve molecules based on molecular size and charge, although in both cases, junctional integrity remains an important mechanism governing transcellular permeability. Despite these highly specialized phenotypes, continuous, discontinuous and fenestrated cells retain an "endothelial" specification.

Adherens junction proteins contribute to the restrictive endothelial cell barrier in each of these cell phenotypes(10), and hence, are important determinants of endothelial specification. Vascular endothelial cell cadherin, VE-cadherin (CDH5), is the principal transmembrane protein comprising an adherens junction(16). VE-cadherin displays a highly restricted expression pattern. It is expressed selectively in endothelium and not in the underlying smooth muscle cells. However, VE-cadherin may not be equally expressed in all endothelial cell phenotypes. For example, VE-cadherin was prominently expressed in

pulmonary arteries, arterioles, and capillaries, but not in venules and veins, in post-mortem human lung(19). In contrast, VE-cadherin reporter mouse models typically reveal a more homogenous expression pattern. A 2.2kb CDH5 promoter sequence was cloned upstream of Cre recombinase and these animals were crossed with various Cre-responsive reporters(18, 24) to engineer constitutive or inducible expression of reporter genes. Approximately half of the endothelial cells isolated from these transgenic mice expressed the reporter gene early in development, and this percentage increased throughout development in blood and lymphatic vessels(18). Near uniform Cre recombinase reporter gene expression was seen in adult endothelium, across multiple organs. The promoter sequence possesses regulatory elements sufficient to drive expression in endothelium while reducing expression in other cell types(18). A similar promoter that also contains a 200.3kb upstream region has been used to drive inducible expression of genes of interest(27, 29, 35, 37, 38) for physiological studies. These studies also confirm the VE-cadherin promoter sequence retains endothelial specificity.

While use of VE-cadherin driven reporter genes has been instrumental in advancing our understanding of endothelial cell fate and properties of angiogenesis and barrier function, mouse models are limited in some areas of vascular biology, especially for the study of chronic lung diseases like pulmonary arterial hypertension(7, 17). In this case, severe pulmonary arterial hypertension is characterized by evolving occlusive neointimal lesions thought to arise from endothelial apoptosis and exuberant hyperproliferation of apoptosis-resistant cells into the lumen. Mouse models of pulmonary arterial hypertension do not typically develop this form of the vasculopathy, with the exception of endothelial and hematopoietic prolyl-4-hydroxylase 2 null mice(7, 17). In contrast, rat models better recapitulate the pulmonary arterial hypertension phenotype characterized by neointimal occlusive lesions(1, 4, 36). Therefore, we sought to develop a transgenic rat model that would enable endothelial cell fate mapping during the evolution of chronic vascular disease states, like occlusive vasculopathies. To develop this model, we engineered the rat VE-cadherin promoter upstream of Cre recombinase and crossed this animal with a Cre-sensitive tdTomato reporter rat. Here, we report the resulting progeny possesses prominent reporter activity across multiple organs, in both males and females.

Materials and Methods

Cloning of the CDH5 promoter from rat endothelium. Generation of CDH5-cre recombinase rats was performed at the Genome Rat Resource Center at the Medical College of Wisconsin under protocols approved by the institutional animal care and use committee. An approximate 2.5kB fragment of the CDH5 promoter was cloned upstream of the codon-optimized HA-tagged Cre (iCre) and this expression cassette was subcloned into a *Sleeping Beauty* (SB) transposon vector(15). The SB method of transpositional transgenesis (TnT) was used to produce transgenic Sprague Dawley (Crl:SD, Charles River Laboratories) rats by pronuclear microinjection as we have previously described(21, 22). Three transgenic founders were produced, one of which demonstrated robust endothelial-specific Cre expression when crossed to the tdTomato Reporter Knock-in Rat (Horizon). This founder was then backcrossed to the parental Crl:SD strain to establish a colony for further development and characterized (herein referred to as CDH5-iCre).

Animal Care. CDH5-iCre x tdTomato transgenic Sprague-Dawley rats were shipped from the Medical College of Wisconsin to the University of South Alabama for this study. Once received, they underwent a 30-day quarantine, after which time, pathogen testing revealed they were all pathogen-free. Until the time of the study, animals were group-housed in micro-isolation caging with enrichment, according to the established guidelines for care and use of laboratory animals. Rooms were on a 12-hour light-dark cycle and temperature was controlled. Sixteen animals were studied, including 10 females and 6 males. Procedures were reviewed and approved by the University of South Alabama institutional animal care and use committee.

Animal surgery and tissue preparation. Tissues and vessels of interest were harvested from transgenic rats to examine the expression and distribution of tdTomato fluorescent protein. For lung tissue, we utilized the agarose/gelatin-infused lung slice technique to evaluate tdTomato fluorescence, autofluorescence, and Hoechst nuclear dye (NucBlue, Invitrogen) fluorescence within a 300 μm thick lung tissue. Rats were sedated with injection of sodium pentobarbital intraperitoneally and an anesthetic

plane was verified by lack of toe pinch response. Rats were then injected with 0.3 mL heparin intraperitoneally and following thoracotomy the pulmonary artery was cannulated through the right ventricle. The left ventricle was nicked, and ~30 mL of Hanks Buffered Saline Solution (HBSS, Gibco) was slowly perfused through the pulmonary circulation. Next, NucBlue (3 mL) was perfused through the pulmonary artery cannula and a stopcock was used to infuse ~15 ml gelatin (6%; ThermoFisher Scientific) solution into the pulmonary circulation. The right lung was then sutured at the hilum, and a tracheal tube was inserted, followed by infusion of ~20 ml agarose (2.7%; ThermoFisher Scientific) solution to inflate the left lung. Ice was used *in situ* to solidify the gel *en bloc*. The left lung, heart and trachea were excised *en bloc* and placed in cold HBSS on ice at 4 ℃ for 1 hr. The left lung was cut using a razor into ~1 mm thick slice at the hilum and then sliced into 300 μm thick serial sections using a vibratome. Slices were added to a six-well, glass-bottom plate (cellvis) and placed in an incubator for 1 hr. An Andor Revolution RS3 (Andor) microscope using IQ (Andor, v3.6.1) software was used to collect z-stacks (100 planes at ~ 0.4 um/plane) of selected structures within the slices using the RSL red (emission: 625 nm), RSL green (emission: 525 nm), and Dapi (emission: 440 nm) filter sets.

Other tissues, including liver, spleen, mesentery and brain, were harvested and placed in buffered saline solution. Tissues were then cut into thin (~0.5 mm) slices using a surgical knife. A representative section of each tissue was incubated with NucBlue (ThermoFisher Scientific) for 60 minutes to visualize nuclei. Blood vessels, including the aorta, carotid artery, jugular vein, inferior vena cava (IVC), and basilar artery, were harvested, cut longitudinally, opened, and pinned onto SYLGARD 182 blocks (182 silicone elastomer, DOW Chemical) as previously described (13). Blocks were then immersed in buffered solution containing NucBlue for 10 minutes. Blocks were washed and placed in a 35 mm round glass culture dish (separated 100 μm from glass by two parallel supporting pins) containing PBS. All tissues and vessels harvested from rats in all three age groups (6-7.5 months, 14-16.5 months, and 17-19.5 months) were prepared similarly. Prepared specimens were imaged using a Nikon A1R confocal microscope (Nikon Instruments).

Hyperspectral imaging. Hyperspectral imaging analysis approaches were utilized to examine the distribution and expression of tdTomato fluorescent protein across a range of tissue types, while accounting for tissue type–specific autofluorescence(12). Hyperspectral z-stack images were acquired using a Nikon A1R confocal microscope and several objectives, including 4X (Plan Apo λ 4X), 20X (Plan Fluor 20X multi immersion DIC N2), and 60X (Plan Apo VC 60X WI DIC N2). Samples (both from transgenic rats and control rats) were excited using 405 nm for NucBlue, 488 nm for autofluorescence, and 561 nm for tdTomato and autofluorescence simultaneously and the emission spectrum was collected using wavelengths ranging from 424 nm – 724 nm in 10nm increments. All 3 laser lines were set to 20% illumination intensity. The z-step (axial) interval for z-stack acquisition was set at 30 μm, 2 μm, and 1 μm, for 4X, 20X, and 60X objectives, respectively. Specimens were imaged first using the 4X objective, and subsequently with 20X and 60X objectives. A confocal pinhole size of 38.3 μm and detector voltage gain of 130 were used. Similar imaging parameters and settings were utilized across all image data acquired. Imaging parameters were selected so as to maximize signal-to-noise ratio while minimizing photobleaching of tdTomato.

A spectral library containing pure spectra of each endmember (tdTomato, NucBlue, and tissue-specific autofluorescence) was generated to analyze spectral image data. To construct the spectral library, spectral images were acquired using HEK 293 cells either transfected with tdTomato or labeled with NucBlue to obtain pure tdTomato and NucBlue spectral signatures, respectively. Tissues and vessel specimens from control Sprague Dawley rats were imaged to obtain tissue-specific spectral signatures. Custom developed MATLAB programs were utilized to linearly unmix raw spectral data into individual endmembers including tdTomato, NucBlue, and tissue autofluorescence. Unmixed images of tdTomato were used to visualize and quantify the expression and distribution of tdTomato fluorescence signal in different conduit vessels and tissues.

Quantitative Analysis. The age-dependent distributions of tdTomato fluorescence signal in the carotid artery and the jugular vein were quantified using ImageJ analysis software(32). Images acquired using a 4X objective were utilized for quantitative measurements. Maximum intensity projection images of

tdTomato and NucBlue signals were generated from unmixed tdTomato and nuclei image z-stacks, respectively. A region of interest was selected to cover the maximum possible area occupied by the vessel while eliminating all areas outside of the vessel, as based on the NucBlue projected image. This region of interest was applied to the tdTomato maximum intensity projected image, and the tdTomato image was subsequently cropped to eliminate any effects from areas outside of the tissue, thus removing any potential bias from blank regions of the image. A lower-bound intensity threshold of 0.2% and 0.3% of maximum signal intensity (grey scale values of 126 and 200 out of 65535) was selected for carotid and jugular images, respectively, to define pixels that were tdTomato positive. The tdTomato positive fractional area of the thresholded image was then calculated. The same lower-bound intensity threshold was applied to all images ($n \geq 4$ rats for each age group) in each group. The age-dependent tdTomato positive fractional area in carotid artery and jugular vein was plotted for each age group. Statistical significance of variations in tdTomato positive fractional area per age group were calculated using one-way ANOVA, with multiple comparisons and Tukey post-hoc test. Significance was established at $p < 0.05$.

Results

The rat CDH5 promoter shares limited homology to the equivalent mouse promoter. The rat CDH5 start site was identified, and the promoter region resolved by alignment against the mouse sequence. The cloned mouse and rat promoters were 2,509 and 2,508 bp, respectively (**Figure 1A, B**). Whereas the previously reported mouse promoter fragment overlaid the first exon by 86 bp, the cloned rat promoter extended 79 bp past the transcription start site. These promoters shared sequence homology, equal to 60% using EMBOSS, 64.4% using Lalign, 64.9% using AlignX (Vector NTI) (**Figure 1C**). In both genes, translation initiation sites are located in the second exon separated by 11,285 bp and 22,923 bp from transcription initiation sites in murine and rat genes, respectively. Therefore, the first intron in the rat gene, while incompletely sequenced at this point, appears to be much larger (22,862 bp *vs* 11,147 bp). Once cloned, the rat promoter was placed upstream of codon-optimized iCre with a HA tag and subcloned into a *Sleeping Beauty* transposon vector for generation of transgenic rats (**Figure 1D**), as described in the *Material and Methods*. Founders were bred and backcrossed into the parental strain to establish the colony. tdTomato fluorescence was tested among the progeny from the colony to assess for rat CDH5 promoter efficacy.

tdTomato fluorescence is limited to the endothelium within the conduit vessel wall. A spectral library containing the unique spectra of each endmember was compiled using image data from single label control samples. Controls for tdTomato and NucBlue were prepared using HEK 293 cells that were either transfected with DNA encoding tdTomato or labeled with NucBlue. Controls for autofluorescence were prepared in an organ and tissue-specific manner. Tissues and vessels from control Sprague Dawley wild-type rats were harvested. Tissues and vessels were prepared and mounted as described in *Materials and Methods*. Spectral images of each single-label control and tissue type were acquired, including tdTomato (**Figure 2A**), NucBlue (**Figure 2B**) and tissue-specific autofluorescence (**Figure 2C**– example from jugular vein autofluorescence). Spectral libraries (**Figure 2D**) containing the unique spectra of tdTomato, NucBlue, and the autofluorescence of the tissue of interest were constructed by extracting the pixel-averaged spectrum from regions of interest in images of control specimens (shown as red, blue and

yellow regions in **Figure 2A-C**). Spectral libraries were then used for spectral analysis to unmix respective signals from each fluorescence signature.

A pixel-by-pixel analysis was performed using custom non-negatively constrained linear spectral unmixing algorithms in the MATLAB programming environment (**Figure 2D**). Raw spectral image data (**Figure 2E**) were unmixed into individual spectral components, called endmembers: tdTomato (**Figure 2F**), NucBlue (**Figure 2G**), and tissue autofluorescence (for example, jugular vein autofluorescence shown in **Figure 2H**) using a spectral library. To examine the distribution of tdTomato signal in 3 dimensions, a projection was created through the unmixed z-stack images (**Figure 2J**). With this 3-dimensional analysis different nuclear orientations were apparent, where overlying endothelial cell nuclei are round and underlying smooth muscle cell nuclei are oblong and oriented at 90 degree angles relative to endothelial nuclei. To assess the total tdTomato signal in the sample, a maximum intensity projection was also created (**Figure 2K** includes autofluorescence and **Figure 2L** does not include autofluorescence). The maximum intensity projection was utilized to visualize the distribution and expression of tdTomato in subsequent figures. For mounted vascular specimens, a rotated 3-dimensional view (**Figure 2M**) was used to confirm that the distribution and expression of tdTomato was confined to the endothelium. As seen in the image, tdTomato fluorescence is limited to the apical side of the vessel wall, along with endothelial cell nuclei, and is not associated with underlying smooth muscle cell nuclei, indicating the rat CDH5 promoter possesses the necessary gene regulatory elements to suppress expression in smooth muscle cells. To better resolve tdTomato fluorescence on a single cell level, high magnification images are shown in **Figure 3**. Here, tdTomato-positive cells are seen adjoining -negative cells. Endothelial nuclei are shown relative to the orientation of blood flow, and the perpendicular orientation of the underlying smooth muscle cell nuclei are visible.

tdTomato fluorescence in the conduit endothelium decreases as animals age. We examined age-dependent distribution of endothelial-restricted tdTomato expression in carotid arteries (**Figure 4**) and jugular veins (**Figure 5**). Similar lookup tables were applied across all unmixed images so that tdTomato intensity was comparable across different image panels. When unmixed overlay images of vessel

preparations obtained at young age (panels **D**, **G**, and **J** in **Figure 4** and **Figure 5**) were compared to images obtained at middle and old age, it was readily observable that the intensity of tdTomato fluorescence in both the carotid artery and jugular vein decreased with age.

tdTomato fluorescence reveals an endothelial cell microheterogeneity within the conduit vessel wall. Images in **Figures 2-5** illustrate a heterogeneous tdTomato fluorescence pattern among endothelial cells within the vessel wall. Examples in **Figures 3, 4J** and **5J** highlight this point, where immediately adjacent cells either did, or did not, display fluorescence. This differential fluorescence pattern signifies an endothelial microheterogeneity based upon the cell's ability to drive iCre expression sufficient to activate the tdTomato reporter. Summary data from 4-6 rats across 3 ages, including young (6-7.5 months), middle (14-16.5 -months) and old (17-19.5-month) age groups, revealed that ≈50% of the vascular surface area was covered by red fluorescence in young animals, and further, that this relative expression pattern decreased significantly in middle- and old-age groups (**Figure 6**). A similar expression pattern, and a similar age-related decrease in tdTomato fluorescence, was observed in both the carotid arteries (**Figure 6A**) and jugular veins (**Figure 6B**). We noted similar tdTomato fluorescence patterns in both male and female subjects. A similar expression of the tdTomato fluorescence signal was observed in other vessel preparations, including the basilar artery, inferior vena cava, and aorta (see **Supplemental Figure 1** at https://doi.org/10.6084/m9.figshare.12461894.

Organ microcirculations exhibit uniform tdTomato fluorescence. We screened various organs for tdTomato fluorescence in the microcirculation, including the mesentery, liver, and spleen (**Figure 7**). In all cases red fluorescence was observed, signifying widespread expression, especially prominent in the microcirculation. This uniform capillary endothelial expression was also visualized in lung capillaries. Here, to better visualize capillaries the circulation was filled with gelatin, the airways were filled with agarose, and lung was cut into ≈300 μm sections prior to imaging. Fluorescence intensity is shown in each channel (**Figure 8A**) and composites reveal extensive tdTomato fluorescence in the alveolar capillaries (**Figure 8B**). In **Figure 8B**, a precapillary arteriole adjacent to the capillary network is negative for tdTomato fluorescence, highlighting endothelial heterogeneity within the microcirculation.

307

Discussion

Here, we report development of a novel CDH5-iCre driven transgenic reporter rat that exhibits exceptional endothelial-selective tdTomato fluorescence. In conduit arteries and veins the reporter is restricted to the endothelium and is not seen in the underlying smooth muscle layer. Endothelium from more than 50% of the vascular surface area possesses reporter fluorescence in the conduit vessels of both males and females. The endothelial microheterogeneity visible within the intimal layer is notable; the reason for such heterogeneity has not been established. Prominent tdTomato fluorescence is seen in the parenchyma of various organs, especially in the lung's microcirculation where occlusive neointimal lesions arise. Yet, in both the conduit vessels and the microcirculations, reporter intensity decreases significantly with age.

While a majority of endothelial cells in conduit arteries and veins express the reporter, tdTomato fluorescence was absent in cell clusters throughout the vessel wall. This differential expression pattern supports the notion of endothelial microheterogeneity, where immediately adjacent cells differ in the tdTomato fluorescence. Clonal niches have been previously reported in conduit blood vessels like the aorta. For example, Schwarz and Benditt identified endothelial cell clonal niches based on thymidine uptake as an estimate of replication rates(33, 34). They found that not all endothelial cells in the vessel wall are replication competent. Rather, proliferation relies on the relatively high replication rates of few cells within clusters. A similar heterogeneity of endothelial cell proliferation was reported in pulmonary arteries and arterioles, especially during the development of pulmonary arterial hypertension. Ki-67 positive endothelial cells are seen in vascular locations that are remodeling to form occlusive lesions(9, 28). A hierarchy of single endothelial cell growth potentials exists among cells isolated from the vessel wall. Single cell cloning of endothelial cells isolated from conduit vessels reveals that few cells are highly replication competent(5, 20, 39). In contrast, endothelial cells isolated from the lung microcirculation exhibit a high proportion of replication competent clones, suggesting it is an enriched endothelial progenitor niche(3); a molecular basis for these proliferative lung capillary endothelial cells has recently been identified(25). It is uncertain whether the presence or absence of tdTomato relates to endothelial cell

proliferative potential, yet this reporter animal provides a way to track endothelial heterogeneity both *in vivo* and *in vitro*.

Endothelial cell dysfunction is a cardinal feature of aging. We report a significant loss of endothelial cell tdTomato fluorescence as the animal ages. Whether this decrease in fluorescence reflects a silencing of tdTomato transcription, an increase in tdTomato turnover or some impairment in the fluorescent property of tdTomato remains to be determined. Nonetheless, it is noteworthy that this decrease in reporter efficacy tracks with the age-dependent loss of VE-cadherin within adherens junctions(8). The loss of VE-cadherin in the adherens junction contributes to both impairment of endothelium-dependent vasodilation(8) and increased permeability(6, 11, 26). Thus, the tracking tdTomato fluorescence as a function of age may provide insight into vascular dysfunction that accompanies the aging process.

In conclusion, we report a first-in-kind endothelial-restricted transgenic reporter rat. Endothelial expression of the tdTomato was ubiquitous in all circulations tested. Whereas a microheterogeneity in tdTomato fluorescence was seen in conduit vessels, the fluorescence pattern was uniform in the microcirculations of various organs, most prominently in the lungs. This transgenic reporter rat represents an ideal model for assessing endothelial remodeling in various chronic vascular disease states, like atherosclerosis and pulmonary arterial hypertension. The model will be useful for acute injury studies, such as ischemic and hemorrhagic stroke, where adherens and tight junctions are disrupted and where blood brain permeability is compromised. It allows for assessment of endothelial injury and repair in the lung, as occurs during infection, where loss of capillary density and angiogenesis or vasculogenesis can be tracked fluorescently. tdTomato fluorescence can be measured alongside other fluorescent macromolecular tracers to assess sites of permeability within the vessel wall. However, tdTomato fluorescence decreases as the animals age, which represents a limitation for its use in aging models. Nonetheless, we anticipate this unique animal resource will have widespread application to physiological studies in vascular biology.

Acknowledgements

This work was supported by HL60024 (T.S., M.A., S.L., T.R., M.T., R.B., D.F.A.), HL66299 (T.S. and M.A.), HL140182 (M.L. and T.S.), HL114474 (A.M.G.), HL116264 (A.M.G.), OD026560 (A.M.G.), HL118334 (D.F.A.), and HL136869 (C.M.F. and T.S.). We would like to thank Dr. Michele Schuler and Leigh Ann Wiggins for their assistance in veterinary care, and Dr. Madhuri Mulekar for her assistance with statistical analysis.

References

1. **Abe K, Toba M, Alzoubi A, Ito M, Fagan KA, Cool CD, Voelkel NF, McMurtry IF, and Oka M**. Formation of plexiform lesions in experimental severe pulmonary arterial hypertension. *Circulation* 121: 2747-2754, 2010.

2. **Aird WC**. Phenotypic heterogeneity of the endothelium: I. Structure, function, and mechanisms. *Circ Res* 100: 158-173, 2007.

3. **Alvarez DF, Huang L, King JA, ElZarrad MK, Yoder MC, and Stevens T**. Lung microvascular endothelium is enriched with progenitor cells that exhibit vasculogenic capacity. *Am J Physiol Lung Cell Mol Physiol* 294: L419-430, 2008.

4. **Alzoubi A, Almalouf P, Toba M, O'Neill K, Qian X, Francis M, Taylor MS, Alexeyev M, McMurtry IF, Oka M, and Stevens T**. TRPC4 inactivation confers a survival benefit in severe pulmonary arterial hypertension. *Am J Pathol* 183: 1779-1788, 2013.

5. **Basile DP, and Yoder MC**. Circulating and tissue resident endothelial progenitor cells. *J Cell Physiol* 229: 10-16, 2014.

6. **Belmin J, Corman B, Merval R, and Tedgui A**. Age-related changes in endothelial permeability and distribution volume of albumin in rat aorta. *Am J Physiol* 264: H679-685, 1993.

7. **Carman BL, Predescu DN, Machado R, and Predescu SA**. Plexiform Arteriopathy in Rodent Models of Pulmonary Arterial Hypertension. *Am J Pathol* 189: 1133-1144, 2019.

8. **Chang F, Flavahan S, and Flavahan NA**. Impaired activity of adherens junctions contributes to endothelial dilator dysfunction in ageing rat arteries. *J Physiol* 595: 5143-5158, 2017.

9. **Cool CD, Kennedy D, Voelkel NF, and Tuder RM**. Pathogenesis and evolution of plexiform lesions in pulmonary hypertension associated with scleroderma and human immunodeficiency virus infection. *Hum Pathol* 28: 434-442, 1997.

10. **Dejana E**. Endothelial adherens junctions: implications in the control of vascular permeability and angiogenesis. *J Clin Invest* 98: 1949-1953, 1996.

11. **Ezekowitz MD, Parker KH, Salpidoru N, and Oxenham RC**. Effect of aging on permeability of cockerel aorta to 125I-albumin. *Am J Physiol* 239: H642-650, 1980.

12. **Favreau PF, Deal JA, Harris B, Weber DS, Rich TC, and Leavesley SJ**. Label-free spectroscopic tissue characterization using fluorescence excitation-scanning spectral imaging. *J Biophotonics* 13: e201900183, 2020.

13. **Francis M, Waldrup JR, Qian X, Solodushko V, Meriwether J, and Taylor MS**. Functional Tuning of Intrinsic Endothelial Ca2+ Dynamics in Swine Coronary Arteries. *Circ Res* 118: 1078-1090, 2016.

14. **Gebb S, and Stevens T**. On lung endothelial cell heterogeneity. *Microvasc Res* 68: 1-12, 2004.

15. **Geurts AM, Yang Y, Clark KJ, Liu G, Cui Z, Dupuy AJ, Bell JB, Largaespada DA, and Hackett PB**. Gene transfer into genomes of human cells by the sleeping beauty transposon system. *Mol Ther* 8: 108-117, 2003.

16. **Giannotta M, Trani M, and Dejana E**. VE-cadherin and endothelial adherens junctions: active guardians of vascular integrity. *Dev Cell* 26: 441-454, 2013.

17. **Gomez-Arroyo J, Saleem SJ, Mizuno S, Syed AA, Bogaard HJ, Abbate A, Taraseviciene-Stewart L, Sung Y, Kraskauskas D, Farkas D, Conrad DH, Nicolls MR, and Voelkel NF**. A brief overview of mouse models of pulmonary arterial hypertension: problems and prospects. *Am J Physiol Lung Cell Mol Physiol* 302: L977-991, 2012.

18. **Gory S, Vernet M, Laurent M, Dejana E, Dalmon J, and Huber P**. The vascular endothelial-cadherin promoter directs endothelial-specific expression in transgenic mice. *Blood* 93: 184-192, 1999.

19. **Herwig MC, Muller KM, and Muller AM**. Endothelial VE-cadherin expression in human lungs. *Pathol Res Pract* 204: 725-730, 2008.

20. **Ingram DA, Mead LE, Moore DB, Woodard W, Fenoglio A, and Yoder MC**. Vessel wall-derived endothelial cells rapidly proliferate because they contain a complete hierarchy of endothelial progenitor cells. *Blood* 105: 2783-2786, 2005.

21. **Ivics Z, Mates L, Yau TY, Landa V, Zidek V, Bashir S, Hoffmann OI, Hiripi L, Garrels W, Kues WA, Bosze Z, Geurts A, Pravenec M, Rulicke T, and Izsvak Z**. Germline transgenesis in rodents by pronuclear microinjection of Sleeping Beauty transposons. *Nat Protoc* 9: 773-793, 2014.

22. **Katter K, Geurts AM, Hoffmann O, Mates L, Landa V, Hiripi L, Moreno C, Lazar J, Bashir S, Zidek V, Popova E, Jerchow B, Becker K, Devaraj A, Walter I, Grzybowksi M, Corbett M, Filho AR, Hodges MR, Bader M, Ivics Z, Jacob HJ, Pravenec M, Bosze Z, Rulicke T, and Izsvak Z**. Transposon-mediated transgenesis, transgenic rescue, and tissue-specific gene expression in rodents and rabbits. *FASEB J* 27: 930-941, 2013.

23. **Mehta D, and Malik AB**. Signaling mechanisms regulating endothelial permeability. *Physiol Rev* 86: 279-367, 2006.

24. **Monvoisin A, Alva JA, Hofmann JJ, Zovein AC, Lane TF, and Iruela-Arispe ML**. VE-cadherin-CreERT2 transgenic mouse: a model for inducible recombination in the endothelium. *Dev Dyn* 235: 3413-3422, 2006.

25. **Niethamer TK, Stabler CT, Leach JP, Zepp JA, Morley MP, Babu A, Zhou S, and Morrisey EE**. Defining the role of pulmonary endothelial cell heterogeneity in the response to acute lung injury. *Elife* 9: 2020.

26. **Oakley R, and Tharakan B**. Vascular hyperpermeability and aging. *Aging Dis* 5: 114-125, 2014.

27. **Okabe K, Kobayashi S, Yamada T, Kurihara T, Tai-Nagara I, Miyamoto T, Mukouyama YS, Sato TN, Suda T, Ema M, and Kubota Y**. Neurons limit angiogenesis by titrating VEGF in retina. *Cell* 159: 584-596, 2014.

28. **Oshima K, Crockett ES, Joshi SR, McLendon JM, Matsumoto Y, McMurtry IF, Abe K, and Oka M**. Aneurysm-type plexiform lesions form in supernumerary arteries in pulmonary arterial hypertension: potential therapeutic implications. *Am J Physiol Lung Cell Mol Physiol* 317: L805-L815, 2019.

29. **Payne S, De Val S, and Neal A**. Endothelial-Specific Cre Mouse Models. *Arterioscler Thromb Vasc Biol* 38: 2550-2561, 2018.

30. **Predescu D, Vogel SM, and Malik AB**. Functional and morphological studies of protein transcytosis in continuous endothelia. *Am J Physiol Lung Cell Mol Physiol* 287: L895-901, 2004.

31. **Predescu SA, Predescu DN, and Malik AB**. Molecular determinants of endothelial transcytosis and their role in endothelial permeability. *Am J Physiol Lung Cell Mol Physiol* 293: L823-842, 2007.

32. **Schneider CA, Rasband WS, and Eliceiri KW**. NIH Image to ImageJ: 25 years of image analysis. *Nat Methods* 9: 671-675, 2012.

33. **Schwartz SM, and Benditt EP**. Aortic endothelial cell replication. I. Effects of age and hypertension in the rat. *Circ Res* 41: 248-255, 1977.

34. **Schwartz SM, and Benditt EP**. Clustering of replicating cells in aortic endothelium. *Proc Natl Acad Sci U S A* 73: 651-653, 1976.

35. **Sorensen I, Adams RH, and Gossler A**. DLL1-mediated Notch activation regulates endothelial identity in mouse fetal arteries. *Blood* 113: 5680-5688, 2009.

36. **Taraseviciene-Stewart L, Kasahara Y, Alger L, Hirth P, Mc Mahon G, Waltenberger J, Voelkel NF, and Tuder RM**. Inhibition of the VEGF receptor 2 combined with chronic hypoxia causes cell death-dependent pulmonary endothelial cell proliferation and severe pulmonary hypertension. *FASEB J* 15: 427-438, 2001.

37. **Wang Y, Nakayama M, Pitulescu ME, Schmidt TS, Bochenek ML, Sakakibara A, Adams S, Davy A, Deutsch U, Luthi U, Barberis A, Benjamin LE, Makinen T, Nobes CD, and Adams RH**. Ephrin-B2 controls VEGF-induced angiogenesis and lymphangiogenesis. *Nature* 465: 483-486, 2010.

38. **Yanagida K, Liu CH, Faraco G, Galvani S, Smith HK, Burg N, Anrather J, Sanchez T, Iadecola C, and Hla T**. Size-selective opening of the blood-brain barrier by targeting endothelial sphingosine 1-phosphate receptor 1. *Proc Natl Acad Sci U S A* 114: 4531-4536, 2017.

39. **Yoder MC**. Is endothelium the origin of endothelial progenitor cells? *Arterioscler Thromb Vasc Biol* 30: 1094-1103, 2010.

Figure Legends

Figure 1. The rat CDH5 promoter was cloned from pulmonary microvascular endothelial cells. Organization of the murine (A) and rat (B) CDH5 genes. The cloned murine and rat CDH5 promoters extend 86 and 79 bp, respectively, beyond corresponding transcription start sites. Translation initiation sites are 11,285 bases and 22,923 bp downstream from the transcription initiation sites in murine and rat primary transcripts, respectively. [C] Alignment of the mouse and rat promoter reveals moderate similarity (from Clustal Omega multiple sequence alignment). [D] Schematic of the piggyback transposon construct. ITR, piggyback inverted terminal repeats; PCDH5, rat CDH5 promoter; attP, PhiC31 recombinase sites; iCre, codon-optimized Cre recombinase; HA, influenza virus hemagglutinin (HA) tag; pA, bovine growth hormone polyadenylation signal.

Figure 2. Spectral library construction and linear spectral unmixing to distinguish tdTomato signal from tissue autofluorescence. False colored images of single label control samples of tdTomato (A), NucBlue (B), and autofluorescence of tissue specimens for each tissue type from Sprague Dawley wild-type rats; a jugular vein is shown as a representative example (C). Spectral libraries (D) were constructed using pure spectra of each endmember that were obtained from selected regions of interest shown in panels A, B, and C. A Representative image from a 3-dimensional image stack (z-stack) of jugular vein acquired at 20X magnification and false-colored by wavelength (E). Spectrally unmixed (non-negatively constrained linear unmixing) images of tdTomato (F), Nuclei (G), and tissue autofluorescence (H) for a given slice in the z-stack. 3-dimensional projections of the raw spectral image stack (I) and false colored (red = tdTomato, blue = NucBlue, green = autofluorescence) unmixed images (J). Maximum intensity projections of unmixed images with (K) and without autofluorescence signals (L). 3-dimensional project highlighting the intima (upper panel of M) and lumen (lower panel of M) of an open vessel. Scale bar = 50 μm.

Figure 3. Single cell tdTomato fluorescence. [A] Unmixed false colored image of the jugular vein vessel preparation (blue = nuclei, green = autofluorescence, and red = tdTomato). White lines indicate the

axis of blood flow through the vessel. The arrowhead highlights the orientation of the oblong endothelial cell nuclei in the foreground that is perpendicular to the underlying and elongated smooth muscle cell nuclei. [B and C] regions of interests shown on panel A (white boxes) are selected to visualize the expression pattern of the tdTomato fluorescence signal in single cells. Scale bar on A, B, and C = 10 μm.

Figure 4. Age-dependent loss of tdTomato fluorescence in the carotid artery. A representative maximum intensity projection of a raw spectral z-stack image acquired using a 4X objective at young (A), middle (B), and old (C) ages. Raw spectral images were unmixed to identify 3 spectral endmembers – tdTomato in red, NucBlue in blue, and autofluorescence in green – and a false-colored merged image is created (D-F). This procedure was also applied for image data acquired with a 20X (G-I) and a 60X objective (J-L). Similar color look-up-tables were used such that the expression intensity is comparable across the images. It is readily observable that the tdTomato fluorescence signal is decreased with aging (compare D to E and F, G to H and I, and J to K and L). White lines in panels A, B and C indicate the axis of blood flow through the vessel. n = 4, 6, and 6 animals for young, middle, and old age groups, respectively.

Figure 5. Age-dependent loss of tdTomato fluorescence in the jugular vein. Maximum intensity projections of the raw spectral image data revealed that the total fluorescence intensity of the tdTomato signal is decreased over age (A, B and C). These results are easily visible by examining the unmixed merged images at 4X magnification (D-F). Similar expression and distribution trends of tdTomato fluorescence were observed when visualized with 20X (G, H, and I) and 60X (J, K, and L) objectives. White lines in panels A, B and C indicate the axis of blood flow through the vessel. n = 4, 6, and 6 animals for young, middle, and old age groups, respectively.

Figure 6. Quantitative assessment of the tdTomato fluorescence signal reveals a decrease with age in both males and females. Fraction area occupied by the tdTomato fluorescence signal is quantified in the carotid artery (A) and jugular vein (B) harvested from young (open circles, male, n = 2, and closed circles, female, n = 2), middle (open squares, male, n = 2, and closed squares, female, n = 4), and old (open triangles, male, n = 2, and closed triangles, female, n = 4) age groups. The percentage of the area

occupied by the tdTomato fluorescence signal (expression) decreased with age in both carotid arteries and jugular veins. * denotes $p < 0.05$ by one-way ANOVA with a Newman-Keuls Multiple Comparison Test.

Figure 7. tdTomato fluorescence is observed among organs. tdTomato fluorescence was seen in the mesentery, hepatic, and spleen microcirculations. In each case detection of the fluorescence was decreased with age.

Figure 8. The pulmonary circulation displays prominent tdTomato fluorescence, particularly in the microcirculation. [A] Fluorescence signals in each of the tdTomato, autofluorescence, and NucBlue channels is shown, with a composite image from young-, middle-, and old-rat age groups. Robust tdTomato fluorescence is seen in the alveolar-capillary endothelium. Fluorescence intensity decreases with age. [B] A composite image reveals uniform tdTomato fluorescence in alveolar-capillary endothelium, although a precapillary arteriole is negative for fluorescence, illustrating heterogeneous cell phenotypes. Scale bar = 50 μm.

[A]

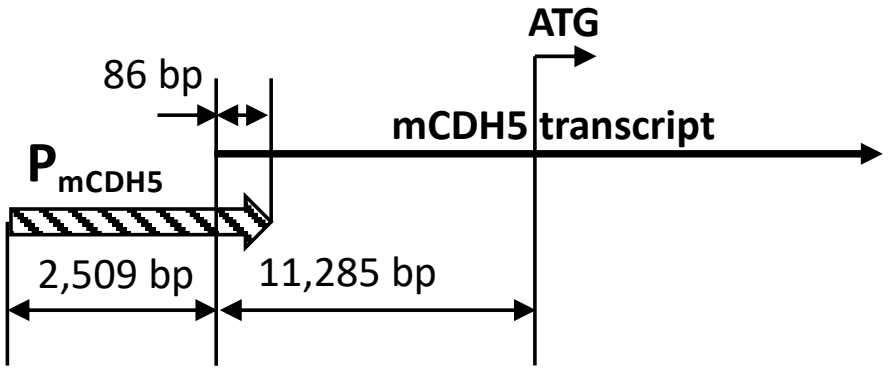

[B]

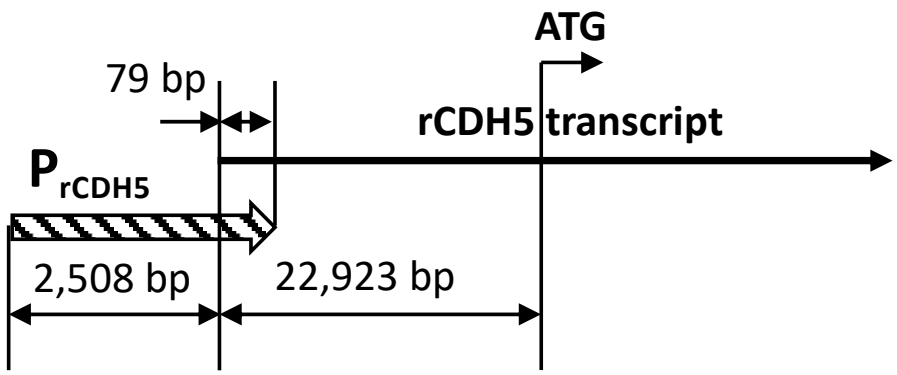

Figure 1

[C]

Figure 1

[D]

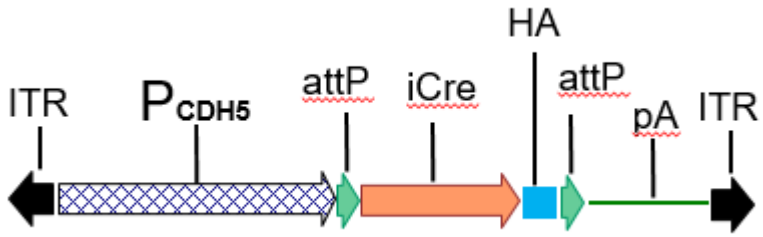

Figure 1

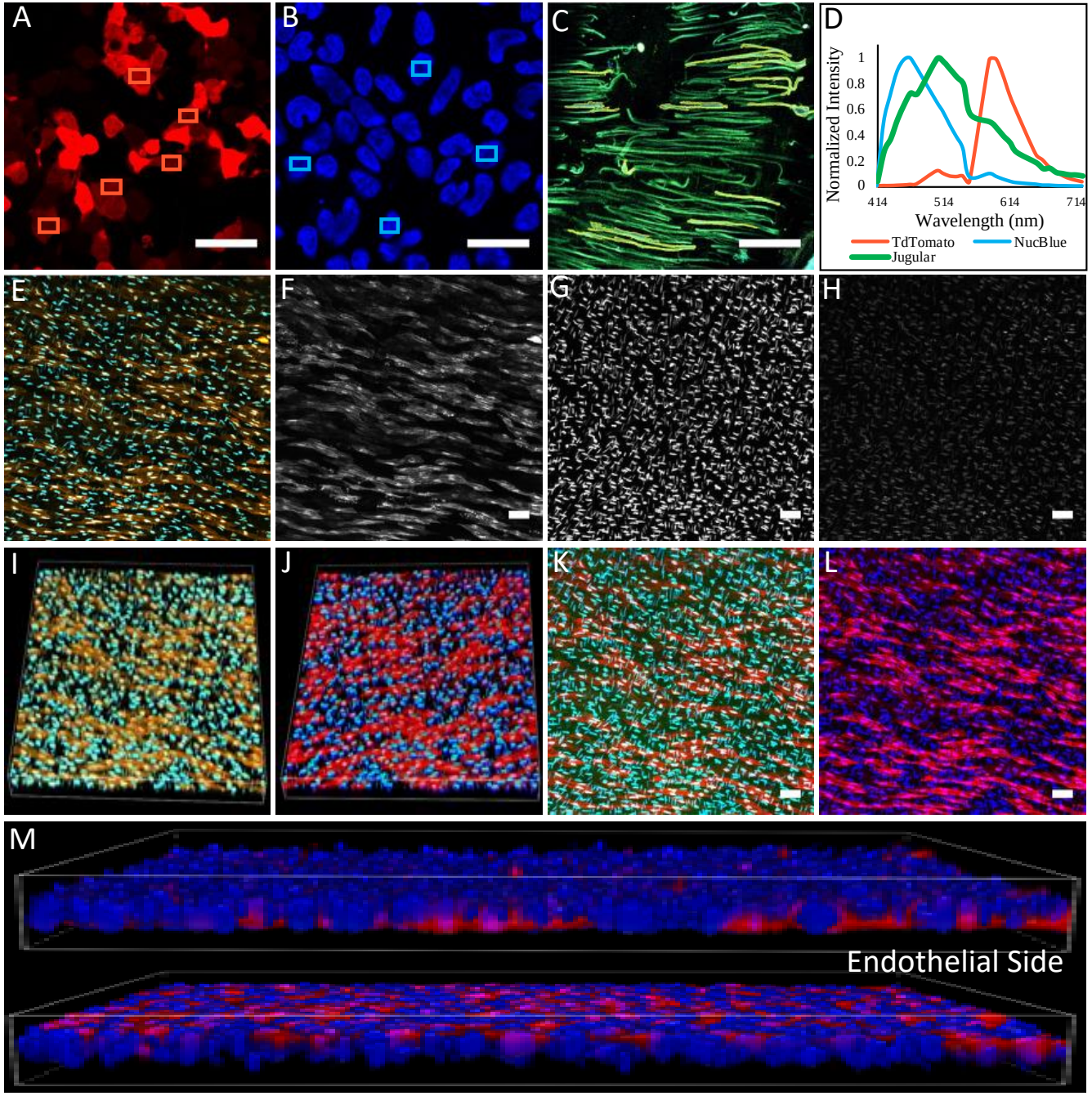

Figure 2

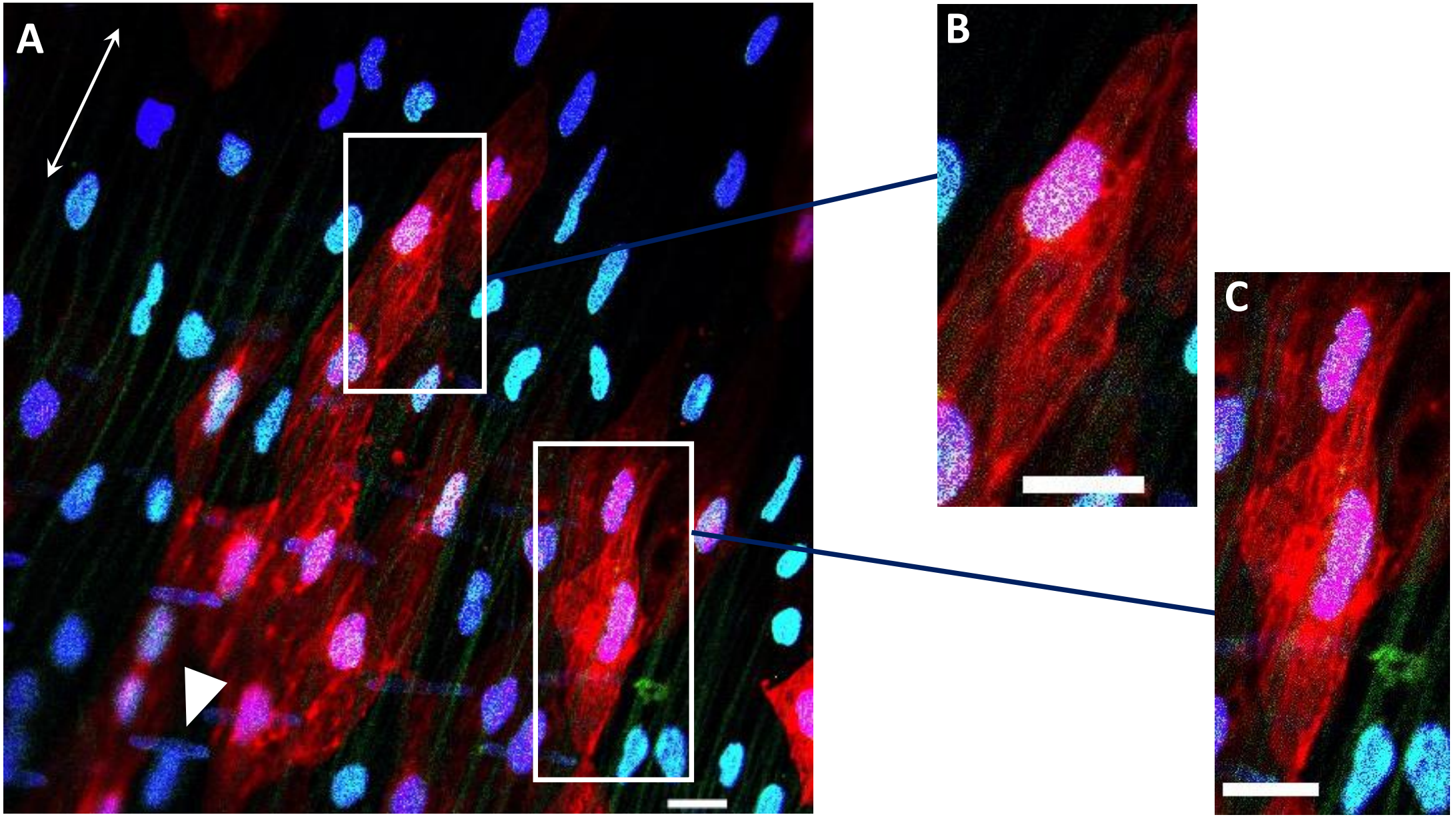

Figure 3

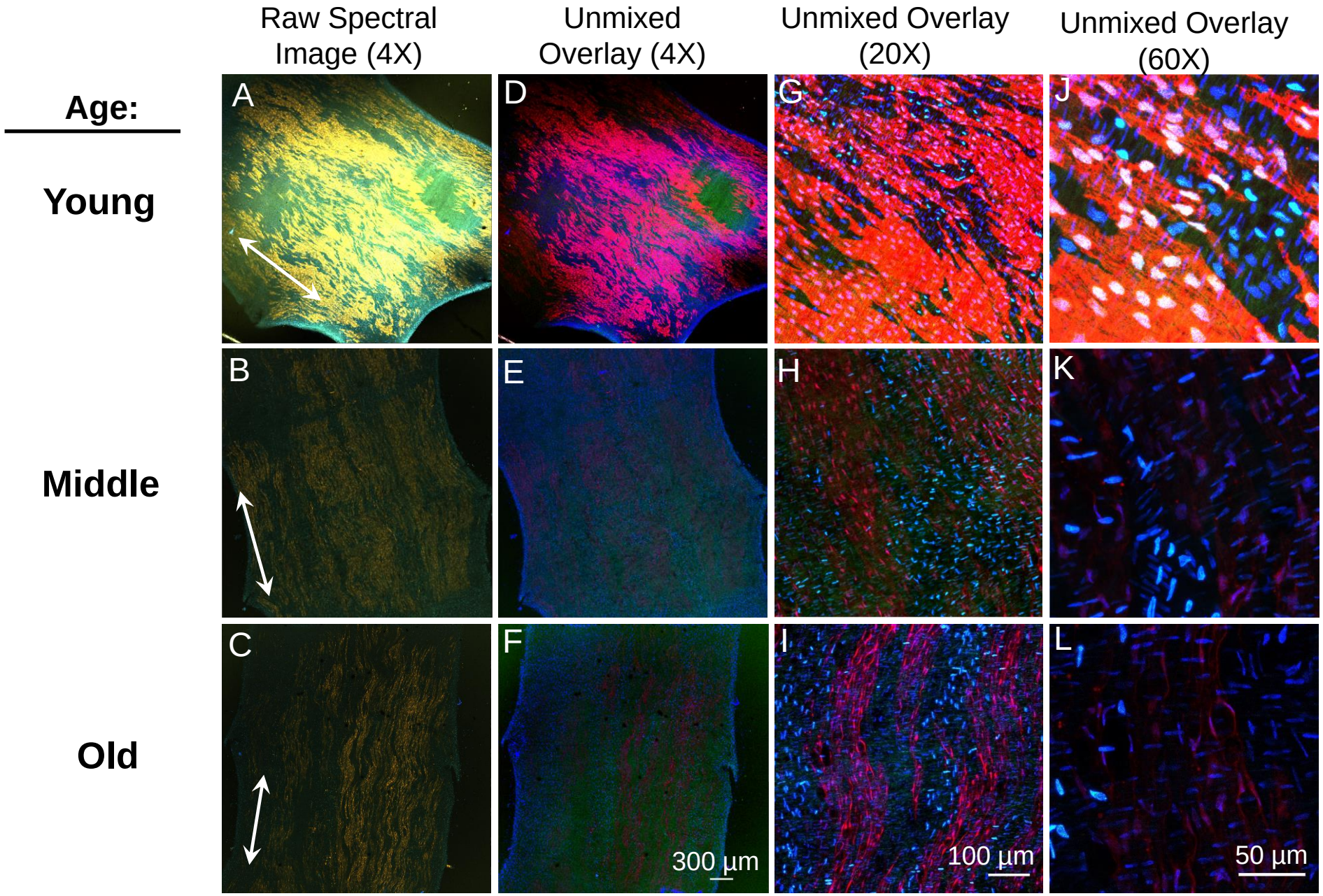

Figure 4

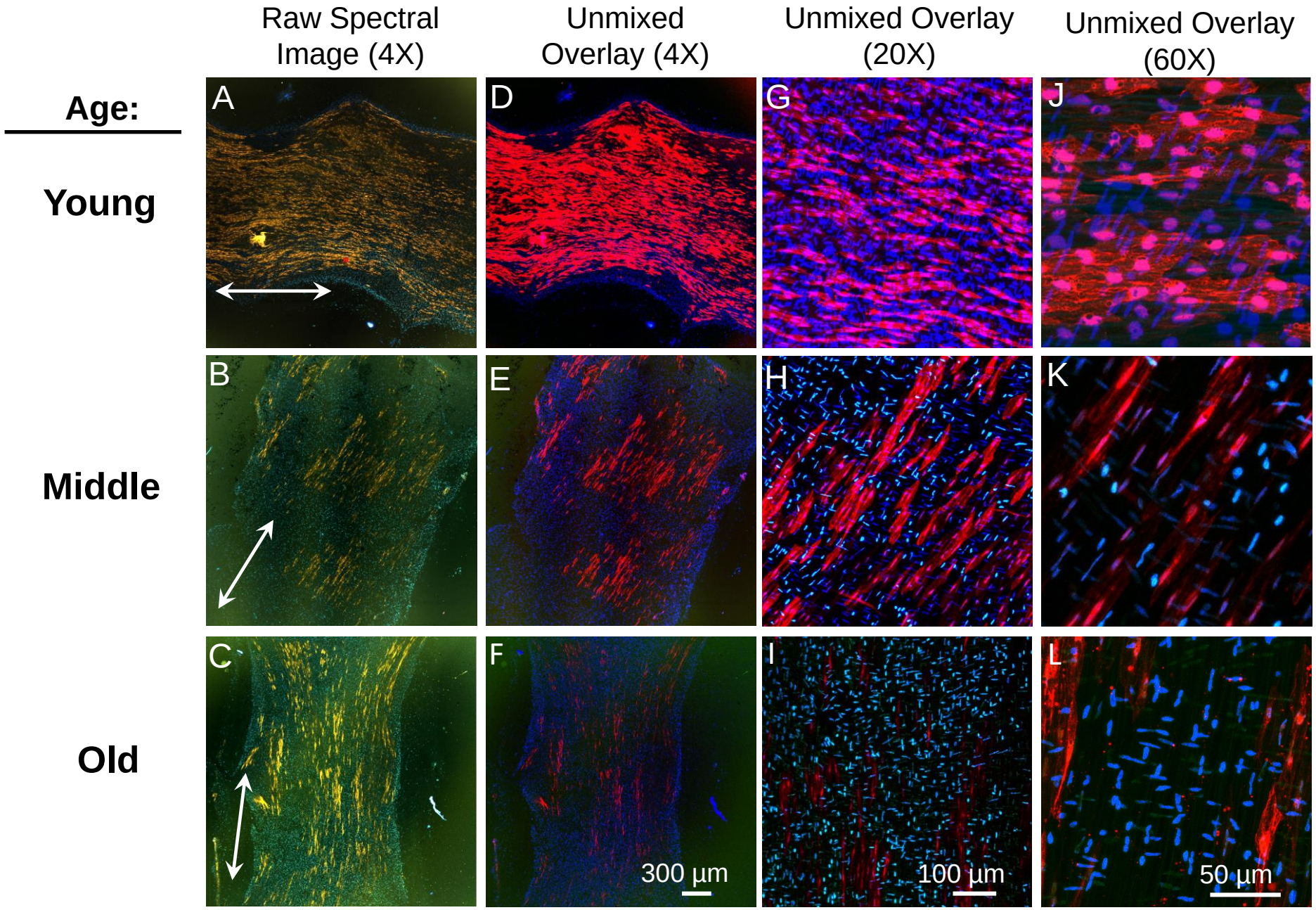

Figure 5

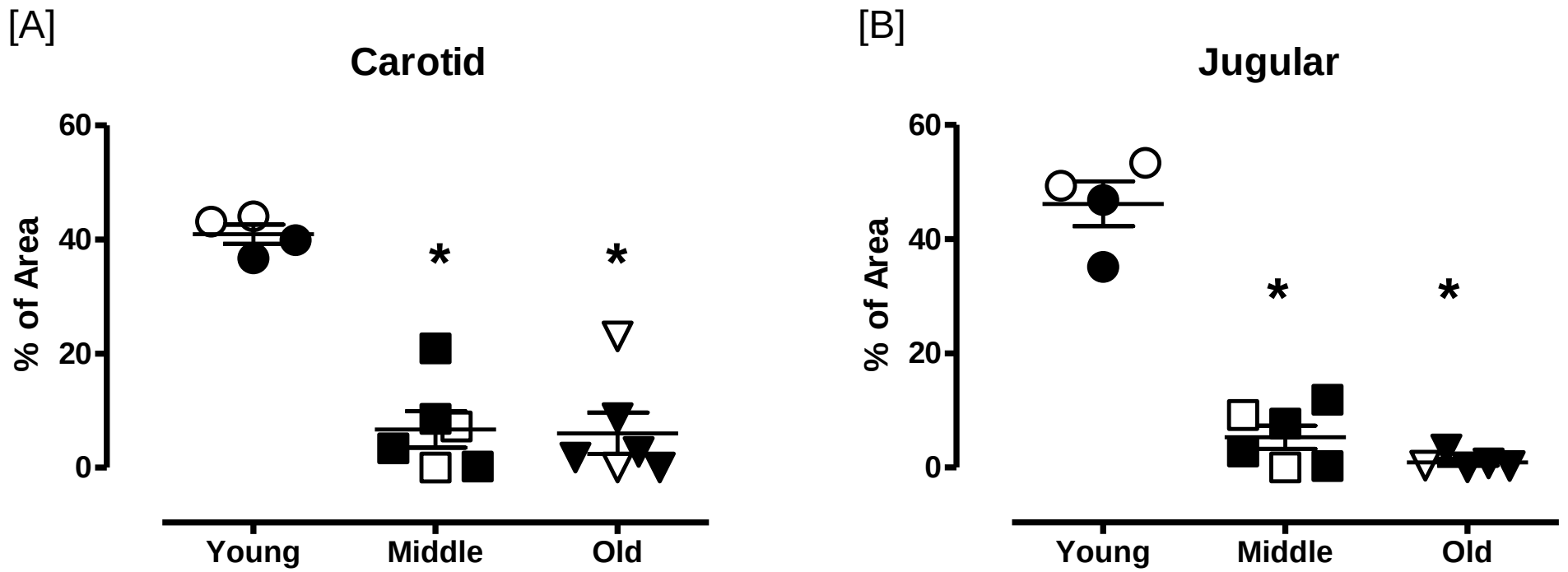

Figure 6

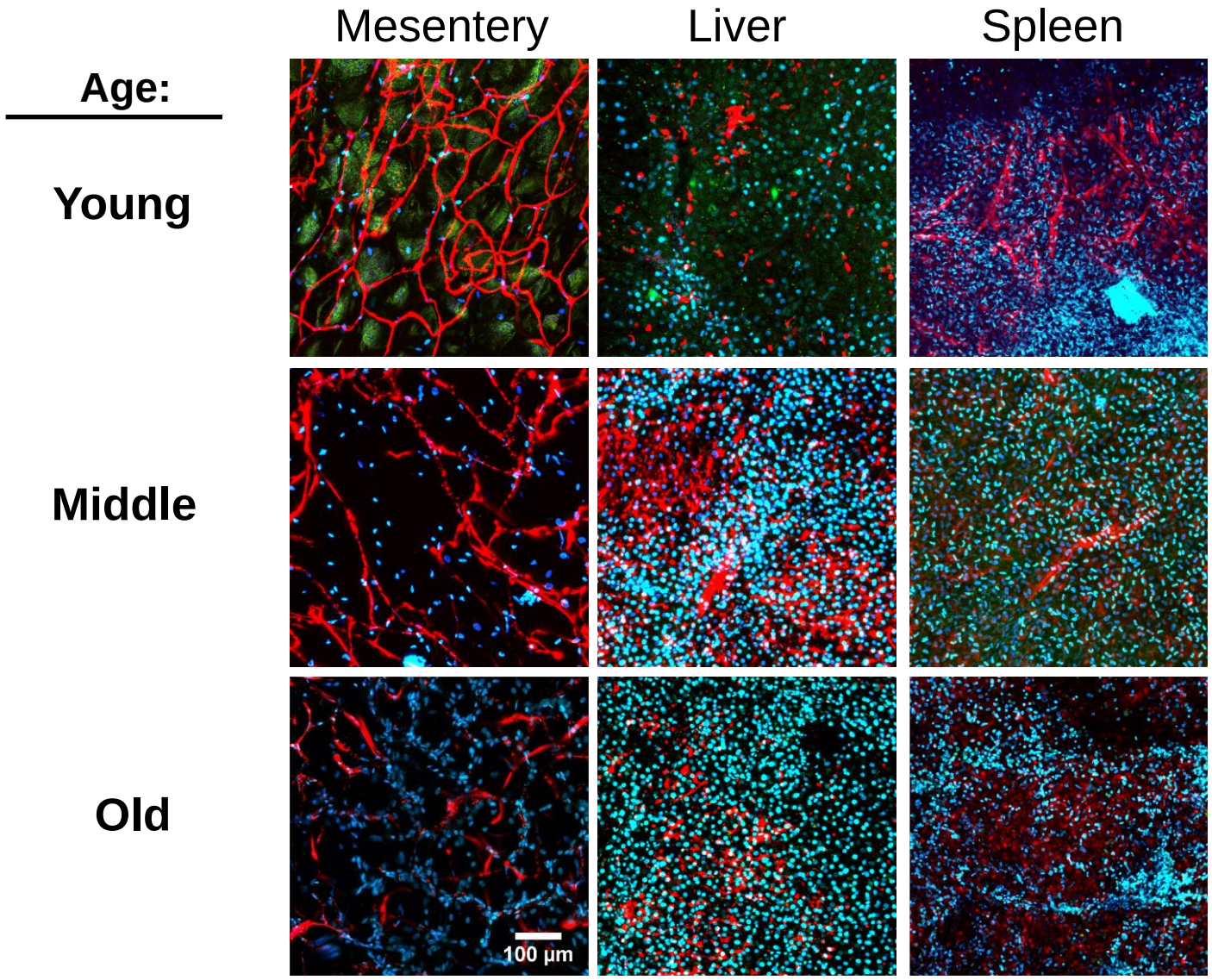

Figure 7

[A]

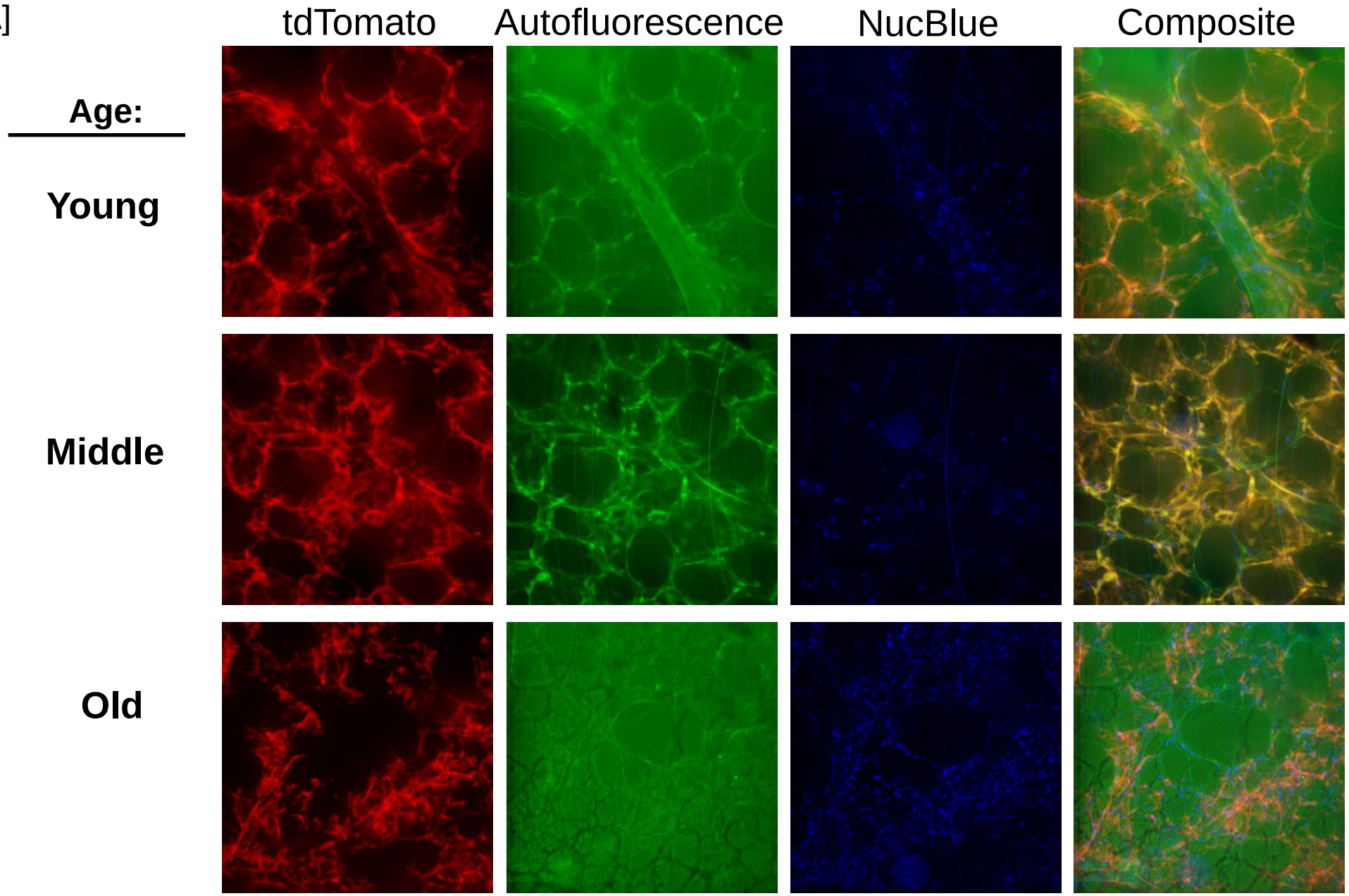

Figure 8

[B]

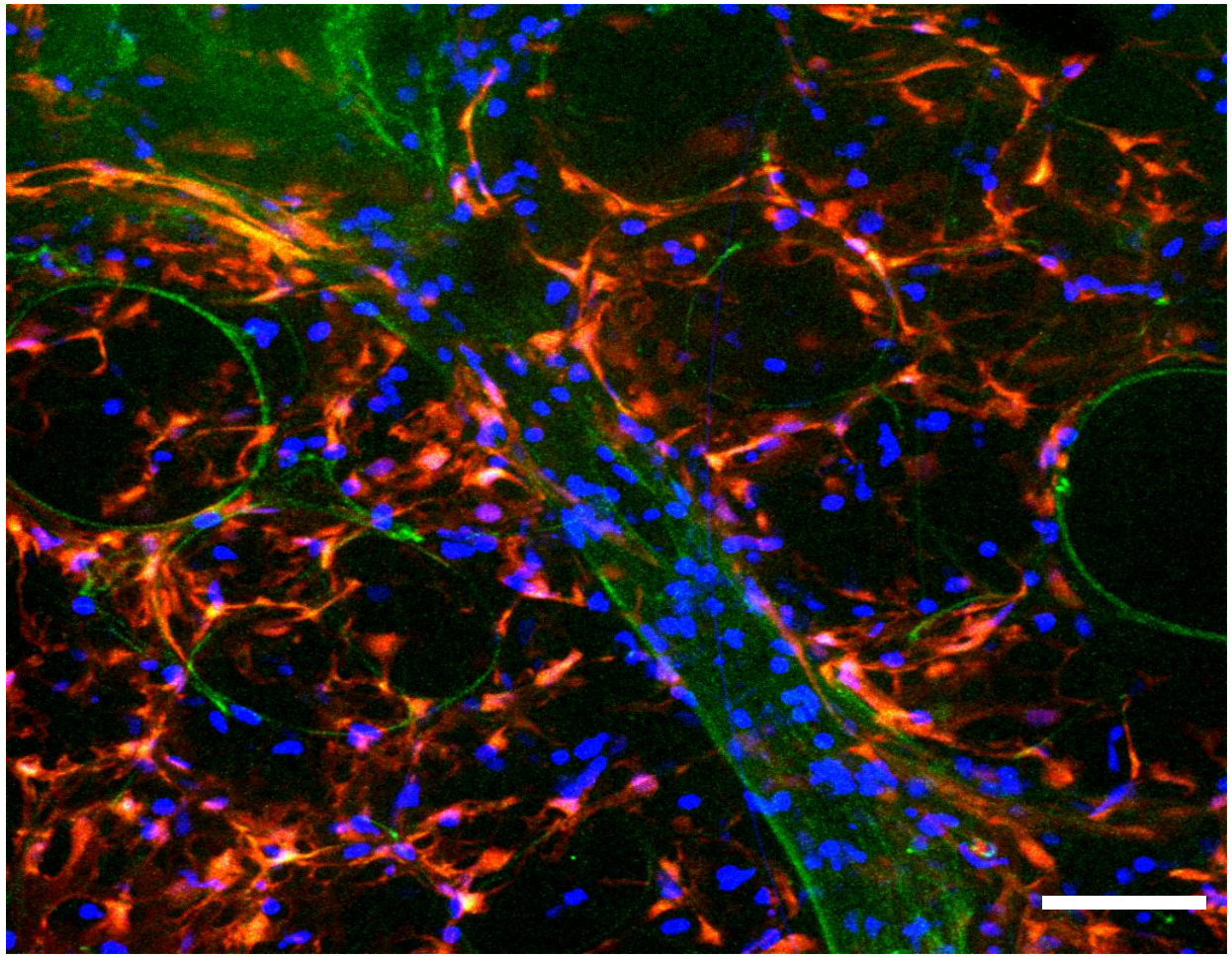

Figure 8